Soil moisture content estimation using ground-penetrating radar reflection data

I.A. Lunt[a,1], S.S. Hubbard[b,*], Y. Rubin[a]

[a]*Department of Civil Engineering, U.C. Berkeley, Berkeley, CA, USA*
[b]*Lawrence Berkeley National Laboratory, MS 90-1116, 1 Cyclotron Road, Berkeley, CA 94720, USA*

Abstract

Ground-penetrating radar (GPR) reflection travel time data were used to estimate changes in soil water content under a range of soil saturation conditions throughout the growing season at a California winery. Data were collected during three data acquisition campaigns over an 80 by 180 m area using 100 MHz surface GPR antennas. GPR reflections were associated with a thin, low permeability clay layer located 0.8–1.3 m below the ground surface that was identified from borehole information and mapped across the study area. Field infiltration tests and neutron probe logs suggest that the thin clay layer inhibited vertical water flow, and was coincident with high volumetric water content (VWC) values. The GPR reflection two-way travel time and the depth of the reflector at the borehole locations were used to calculate an average dielectric constant for soils above the reflector. A site-specific relationship between the dielectric constant and VWC was then used to estimate the depth-averaged VWC of the soils above the reflector. Compared to average VWC measurements from calibrated neutron probe logs over the same depth interval, the average VWC estimates obtained from GPR reflections had an RMS error of 0.018 $m^3\,m^{-3}$. These results suggested that the two-way travel time to a GPR reflection associated with a geological surface could be used under natural conditions to obtain estimates of average water content when borehole control is available and the reflection strength is sufficient. The GPR reflection method therefore, has potential for monitoring soil water content over large areas and under variable hydrological conditions.
© 2004 Published by Elsevier B.V.

Keywords: Soil moisture; GPR; Reflection; Irrigation; Precision agriculture

1. Introduction

Soil moisture content information is needed for studies across a variety of disciplines, such as hydrology, soil science, ecology, meteorology and agronomy. The accuracy and resolution of soil moisture estimates depends on the particular application and associated spatial scale of interest. For example, monitoring the spatial variability of soil

* Corresponding author. Tel.: +1 510 486 5266; fax: +1 510 486 5686.
  E-mail address: sshubbard@lbl.gov (S.S. Hubbard).
[1] Present Address: Department of Earth Sciences, University of Leeds, Leeds, West Yorkshire LS2 9JT, UK.

moisture content with sub-meter resolution over time is important for effective agricultural irrigation, particularly in water-deprived regions with high value crops, such as premium winegrapes. As wine-grape quality is strongly linked to available water and associated soil texture (Jackson, 2000), precision monitoring of soil water content within a vineyard could lead to increased agricultural competitiveness as well as increased water use efficiency.

Variations in soil texture, topography, crop cover and irrigation practices result in large spatial and temporal variability in soil moisture (Western and Grayson, 1998; Huisman et al., 2002; Grote et al., 2003). For example, Western and Grayson (1998) reported that volumetric water content (VWC) associated with the uppermost 0.3 m of the subsurface varied by more than $0.15\ m^3\ m^{-3}$ over tens of meters under wet conditions. Similarly, Huisman et al. (2002) found that soil water variations up to $0.06\ m^3\ m^{-3}$ could be detected at distances larger than 5 m. Although the spatial variability of VWC may be characterized using large numbers of closely spaced conventional measurements, this is generally too time-consuming (Western and Grayson, 1998), and may disturb the soil structure, prohibiting accurate in situ VWC measurements. Airborne imagery can also be used to estimate soil moisture content with meter-scale resolution (e.g. Johnson et al., 2000), but only to a depth of 0.05 m in non-leafy vegetated areas, which is not appropriate in agricultural sites. Rapid and reliable methods of measuring shallow soil moisture content over time and with sufficient spatial density are not readily available. Conventional VWC measurement methods at these small scales include gravimetric, frequency- and time-domain reflectometry (FDR and TDR), neutron probe and capacitance probe techniques. These methods are invasive and provide only limited spatial coverage. Below, we describe three of these conventional techniques for estimating VWC, which are used in our study, followed by a discussion of GPR methods for estimating VWC.

Gravimetric sampling involves extraction of small diameter cores, which are weighed, dried for 24 h at 105 °C according to ASTM D2216, and re-weighed to determine the mass of water in the original sample. The gravimetric water content (GWC) is calculated by dividing the mass of water by the mass of dry soil.

VWC is defined as the ratio of the volume of free water in a soil per unit sample volume, and is related to GWC by (Gardner, 1986):

$$VWC = GWC\rho_d \qquad (1)$$

where ρ_d is the bulk soil density. Although the gravimetric method is simple and accurate, it is time consuming, invasive and labor intensive.

The TDR technique measures the effective dielectric permittivity of the soil over probe length (0.08–2.5 m) (Ferre et al., 1998). The dielectric permittivity of the soil, averaged over the length of the probe, can then be converted to VWC using a site-specific empirical or semi-theoretical equation. TDR probes provide shallow VWC estimation at point locations, and may suffer errors due to air gaps between the soil and the TDR probes (Sakaki et al., 1998; Ferre et al., 1998), or uncertainty in the automatic travel-time measuring technique used by the instrument (Evett, 2000).

The neutron probe log is a borehole technique that can provide one-dimensional measurements of water content to depths of many meters at a single location. The instrument detects the number of backscattered neutron particles in the soil surrounding the borehole, which is proportional to the number of hydrogen ions within the sample volume (Greacen et al., 1981). Hydrogen ions in agricultural soils are present in the form of free water and constituent water. Free water is located in pore spaces between soil particles, and constituent water is the water that occurs within hydrous clay minerals. Greacen et al. (1981) provided calibration equations for loamy soils that can used to estimate $VWC_{constit}$ from the weight percent clay content measured from soil samples

$$VWC_{constit} = \rho_d(0.124\,(wt\%\ clay) + 0.015) \qquad (2)$$

The number of backscattered neutron particles may then be calibrated to the total VWC of the soil. As GPR methods primarily detect free water in soils (Knoll, 1996), in our study, the constituent water contribution is removed in order to convert neutron probe counts to free VWC. The measurement volume of the neutron probe varies with the source and wellbore casing employed as well as with the soil texture and moisture (Keys, 1989), and is approximately a sphere with a radius of 0.3 m (Gardner, 1986). As such, the neutron

probe counts measured near the ground surface are influenced by the air-ground interface and are unreliable. The large sample radius of the neutron probe can also lead to smoothing of sharp changes in the true soil water profile.

Evett (2000) compared the accuracy of the neutron probe, capacitance probe and TDR measurements of VWC at an agricultural test site. The most accurate of these conventional VWC measurement techniques at depth was found to be the neutron probe (RMS error$= 0.009$–0.02 m^3 m^{-3}). The capacitance probe was reported to have an RMS error of around 0.03 m^3 m^{-3} (Evett and Steiner, 1995; Van Overmeeren et al., 1997). Although the error associated with these conventional techniques is acceptable for most applications, the greatest limitation of these techniques is that they sample VWC at a single location only and are not capable of capturing information about field-scale moisture content variability with good spatial resolution and without disturbing the soil. Although a combination of these techniques may be used to estimate the spatial variability of near surface VWC over small areas, any one of these methods is insufficient on its own.

As recently summarized by Huisman et al. (2003), a variety of ground-penetrating radar (GPR) methods have been used to estimate VWC. In GPR studies, the travel time associated with an electromagnetic wave traveling between a radar transmitter and receiver is measured and used to estimate the dielectric permittivity of the soil. Using a site-specific or general empirical relationship (i.e. Topp et al., 1980; Herkelrath et al., 1991) the dielectric permittivity estimates can be converted to VWC estimates. VWC estimates have been obtained using GPR cross-borehole, groundwave and reflection methods. Cross-borehole radar tomography uses the travel time of the radar wave between points of known location to generate a two-dimensional velocity image between the boreholes, which can then be converted to dielectric permittivity and VWC estimates (Hubbard et al., 1997; Binley et al., 2001; Peterson, 2001; Alumbaugh et al., 2002). Alumbaugh et al. (2002) showed that VWC estimates obtained from cross-hole GPR have an RMS error of 0.03 m^3 m^{-3}, when compared with neutron probe estimates of VWC. Cross-borehole surveys are useful in that they can provide a two-dimensional image of VWC up to depths of many

meters. However, their maximum lateral extent is generally less than 10 m, making them mostly useful for small-scale investigations.

GPR groundwave data have been used for accurate estimation of soil water content of the shallow soil at decimeter horizontal resolution (Du and Rummel, 1996; Huisman et al., 2001, 2002, 2003; Hubbard et al., 2002; Grote et al., 2003). As shown in Fig. 1, the transmitted electromagnetic groundwave energy passes directly through the soil to the receiving antenna with a velocity determined by the dielectric permittivity of the soil. VWC was estimated using the groundwave method with a RMS error of 0.011–0.017 m^3 m^{-3} for 900 and 450 MHz antennas, respectively (Grote et al., 2003), and 0.024 m^3 m^{-3} for 225 MHz antennas by Huisman et al. (2001). The depth of influence is a function of soil type and GPR antenna frequency, and was found to be less than 0.2 m in these studies.

Common-mid point (CMP) surveys have also been used by many investigators (Fisher et al., 1992; Greaves et al., 1996; Van Overmeeren et al., 1997; Weiler et al., 1998) to estimate radar wave velocity, and subsequently VWC. In CMP surveys, the transmitter and receiver are moved apart at equal distances from a central location. The travel times of the airwave and groundwave are successively longer as the antenna separation increases, and are represented as dipping reflections with slope equal to the radar wave velocity. Horizontal reflecting surfaces occur as hyperbolic reflections on the resulting GPR plot, the geometry of which can be used to estimate the radar wave velocity. A non-horizontal reflection will not give rise to a true hyperbola on the CMP
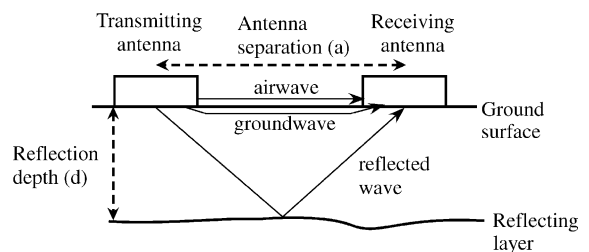

Fig. 1. Schematic diagram showing the GPR antennae and travel path of airwave, groundwave and reflected energy. Antenna separation and reflection depth are used in the calculation of radar wave velocity.

profile (Baker, 1998). Analysis of a CMP survey gives rise to a one-dimensional vertical velocity profile at the location of the CMP. In general, the time required to collect CMP data makes this approach prohibitive for estimation of VWC over large areas and the error associated with CMP velocity analysis is typically on the order of 10% (Tillard and Dubois, 1995; Greaves et al., 1996).

Studies investigating the use of common-offset GPR reflection data for VWC estimation have been conducted only under controlled conditions (i.e. Ulrikson, 1982), where the reflector is artificial and located at a known depth. GPR reflection profiles are collected by moving the transmitting and receiving antennas across the ground surface at a fixed offset, as shown in Fig. 1, and using the travel time to the reflection arrivals to determine the average VWC to the reflector. Grote et al. (2002) used the known depth of buried metal plates in a constructed sand pit to estimate water content to within $0.01 \ m^3 \ m^{-3}$ as compared with gravimetric water content measurements. Stoffregen et al. (2002) estimated VWC from the travel-time of a 1000 MHz GPR wave reflected from the bottom of a lysimeter with a standard deviation of $0.01 \ m^3 \ m^{-3}$.

Our study investigates the accuracy of the common-offset surface GPR reflection method for mapping spatially variable water content, over space and time and under naturally heterogeneous conditions at a California winery. Use of reflection data permits estimation of VWC at the same horizontal resolution provided by surface GPR groundwave techniques (Huisman et al., 2002; Hubbard et al., 2002; Grote et al., 2003), but to greater depths. The radar wave velocity is related to the VWC of the soil and thus, changes in the soil moisture content over time will lead to changes in the two-way travel time (TWTT) and velocity of reflected radar waves. If the reflector depth is known (i.e. from borehole data), GPR reflection TWTT measurements can be used to estimate the averaged VWC of the soil above the reflector. If the depth of the reflector can be estimated (i.e. by interpolation) away from the wellbore measurements then GPR reflection methods have the potential to provide VWC estimates over large areas.

Section 2 describes the use of GPR travel time data for estimating soil water content. Section 3 describes the details of the field area and methods used in this study. Section 4 focuses on the results and the accuracy

of the GPR-derived volumetric water content estimates at the borehole locations under a range of subsurface moisture conditions.

2. GPR background

GPR is a geophysical technique that uses electromagnetic energy with central frequencies generally between 50 and 1200 MHz to image the subsurface. Electromagnetic energy propagates from a transmitting antenna, and is modified by subsurface contrasts in dielectric permittivity (κ) and magnetic permeability (μ). As most soils have negligible variation in magnetic permeability (Powers, 1997), κ has the most significant impact on the recorded GPR response. Some of the electromagnetic energy passes directly from a transmitting to receiving antenna through the air, and is known as the airwave. Part of the transmitted energy, known as the groundwave, propogates through the soil along the ground-air interface to the receiving antenna, and part of the transmitted energy is reflected back to the receiving antenna from subsurface contrasts in dielectric permittivity (Fig. 1).

By knowing the travel path length of the radar wavefront, the electromagnetic wave velocity can be estimated from the direct travel time of the groundwave or the TWTT of the reflected wave. For low-loss media (i.e. soils with low salinity and clay content), the velocity (v) of the soil can be related to the dielectric constant by

$$\kappa = \left(\frac{c}{v}\right)^2, \tag{3}$$

where c is the electromagnetic wave velocity in free space (Davis and Annan, 1989).

GPR reflections are caused primarily by vertical differences in the dielectric properties of the soil. The effective dielectric permittivity κ of a material that has many components (i.e. air, water, soil) can be described using a mixing model

$$\kappa = \left[(1 - \eta)\sqrt{\kappa_s} + (\eta - \text{VWC})\sqrt{\kappa_a} + \text{VWC}\sqrt{\kappa_w}\right]^2, \tag{4}$$

where η is the soil porosity, VWC is the free soil water content and κ_s, κ_a and κ_w are the dielectric permittivities of soil, air and water, respectively (Roth et al., 1990). In unsaturated soils, variations in

soil moisture content have the most significant effect on the subsurface dielectric permittivity. This is because the dielectric permittivity of water (κ_w) over the GPR frequency range is $\sim$81, whereas the dielectric permittivity of air (κ_a) is 1, and that of most soils (κ_s) is between 4 and 7 (Davis and Annan, 1989). Therefore, changes in the volume percentage of water will dominate changes in the effective dielectric permittivity of the soil.

In addition to using mixing models, as described in Eq. (4), estimation of VWC from measurements of κ may also be carried out using petrophysical relationships, such as an empirically derived expression given by Topp et al. (1980), or a semi-theoretical expression given by Herkelrath et al. (1991). Once the velocity of the electromagnetic wave is determined from analysis of the GPR data, it can be used to estimate the dielectric constant using (3), and subsequently to estimate VWC.

The strength of a GPR reflection is a function of the contrast in κ across the reflecting boundary, and is given by the reflection coefficient (RC)

$$ \text{RC} = \frac{\sqrt{\kappa_U} - \sqrt{\kappa_L}}{\sqrt{\kappa_U} + \sqrt{\kappa_L}}, \tag{5} $$

where κ_U is the dielectric permittivity of the upper soil horizon, and κ_L is the permittivity of the lower soil horizon (Davis and Annan, 1989). Given that water has the highest dielectric permittivity of materials commonly found in soils, GPR reflections observed in shallow soils can be caused by vertical contrasts in soil water content (Tsoflias et al., 1999; Kowalsky et al., 2001; Martinez and Byrnes, 2001). Changes in soil texture alone are typically not capable of giving rise to large reflection coefficients (Van Dam and Schlager, 2000; Martinez and Byrnes, 2001) but may be associated with vertical changes in VWC because of different water retention properties of adjacent soils (Saxton et al., 1986; Chan and Knight, 2001; Van Dam et al., 2003).

The thickness of the soil layer relative to the GPR signal wavelength (λ) must also be considered when using GPR reflection data to estimate VWC. Where the vertical VWC varies greatly over short distances, large changes in reflection coefficient may occur over distances less than the GPR wavelength, causing constructive and destructive interference of the GPR response (Van Dam et al., 2003). It is generally assumed that variations in dielectric constant at vertical spacings of less than $\lambda/4$–$\lambda/3$ will not be individually resolved (Annan et al., 1991; Huggenberger, 1993). However, layers thinner than $\lambda/4$ have been resolved on GPR profiles where the reflection coefficient is large (Clement et al., 1997; Van Dam et al., 2003). Chan and Knight (2001) proposed two different methods to determine the depth-averaged vertical variation in κ depending on the ratio of layer thickness (t) to signal wavelength (λ). When $t/\lambda > 10$, Chan and Knight (2001) suggested that the arithmetic average of κ represented the GPR response, and when $t/\lambda < 1$, the geometric average of κ was more appropriate. More information about GPR methods for hydrogeological studies is given by Annan (2005).

3. Study area and methods

3.1. Site description

The study was carried out at the Dehlinger Winery in Sonoma County, CA. Vineyard soils are composed of a 1.5–1.8 m thick red, fine-loamy soil (Sebastopol series) that overlies a buff-colored, clayey soil (Goldridge series; Miller, 1972). Within our 80 by 180 m study area (Fig. 2), soil textures vary between sandy loam and clay loam, but are generally composed of sandy clay loam. Up to 30 wt% gravel is present in the Sebastopol Series soil, but gravel is absent in the Goldridge Series soil. Topography varies by up to 3.5 m over the study area, with the highest elevations in the north-western corner, as shown by the dashed lines in Fig. 2. The water table is approximately 4 m below the ground surface, as measured in nearby wells. Average air temperatures vary between 7 °C between November and March and 16 °C for the remainder of the year. Mean annual precipitation is around 1000 mm, with the majority of the rain falling between November and March. Vines are spaced at 2.44 m (8 ft) intervals and are arranged in rows that are 3.48 m (10 ft) apart: the locations of grapevines are indicated by the small dots on Fig. 2. Metal trellises are located at every fourth vine. No inrow tilling has been performed, and there is no irrigation system, although an above-trellis spray system is infrequently used during hot weather.
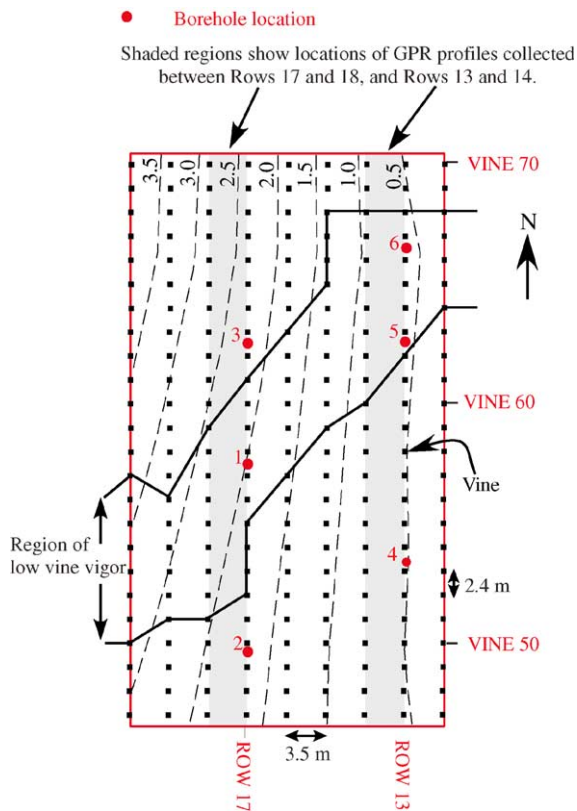
Fig. 2. Map showing locations of boreholes and GPR profiles collected adjacent to rows 13 and 17. Individual vines are represented by dots, and region of low vine vigor is indicated by solid line. Dashed lines are 0.5 m topographic contours. Elevation datum is the lowest point in the study area.

The crops in our study area are 20-year-old Chardonnay vines, all of which are derived from the same rootstock. Vineyard managers monitor the fruit and pruning weight of the vines every year, and have identified a region that displays low vine vigor (low vegetative growth) trending NE–SW across our study area, as indicated on Fig. 2. This study site was chosen because we suspected that variations in vine vigor within areas of identical rootstock might be controlled by natural heterogeneity in soil texture and associated VWC. This study focuses on assessing the accuracy of the GPR reflection method for estimating subsurface VWC over the depth of the root zone, which is generally considered to be the upper $1-2$ m of the soil (Jackson, 2000).

3.2. Data acquisition

Three field campaigns were conducted to provide information about soil moisture conditions during dry (October), intermediate (November), and wet (April) conditions The arrows on Fig. 3 illustrate the timing of the data acquisition campaigns relative to precipitation between August 2002 and June 2003. Precipitation was measured at the California Irrigation Management Information System (CIMIS) station in Santa Rosa, which is approximately four miles from the field site and experiences similar precipitation rates. During each field campaign, neutron probe logs, TDR measurements, soil samples for gravimetric and soil texture analysis, and GPR profiles were collected. Surface sediment samples were also collected every 5–10 m laterally and to a depth of 0.15 m to determine shallow soil texture and bulk density. Topography of the study site was measured using a leveler and surveying rod. Boreholes were augered to a depth of 3.6 m (12 ft) below ground surface and cased with 0.1 m diameter PVC. The locations of boreholes used in this study are shown on Fig. 2. Soil samples within the borehole (sample volume ~ 500 cm^3; sample length 0.1 m) were collected every 0.33 m for texture and gravimetric moisture content measurement. The sediment texture of each borehole soil sample was measured for weight percent sand, silt and clay, and in some cases, weight percent gravel. The bulk density (ρ_d) of each borehole and surface soil sample was
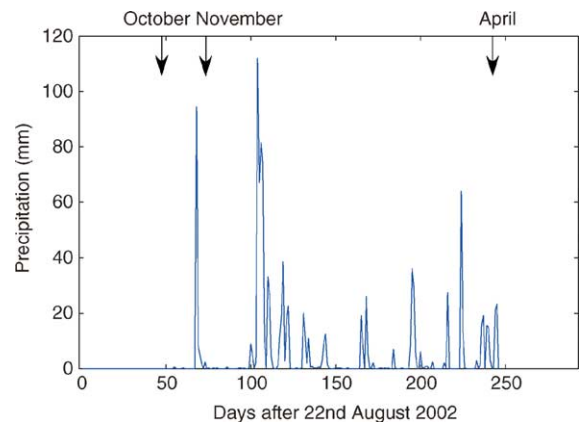

Fig. 3. Precipitation data measured in Santa Rosa, 4 miles from the Dehlinger winery. Arrows indicate timing of data collection campaigns.

calculated from soil texture data (Saxton et al., 1986) and varied between 1.36 and 1.71 g cm^{-3}. Bulk density estimates were used to convert gravimetric to volumetric water content following (1). Where soil samples were not available, a density of 1.5 g cm^{-3} was used. Each borehole was logged immediately after drilling using a CPN 503DR neutron probe with a vertical sampling interval of 0.1–0.2 m.

Common-offset GPR reflection profiles were collected at a central frequency of 100 MHz using a pulseEkko 100 during October and November of 2002, and April of 2003. Reflection profiles were 56 m long, and were collected along 8 rows, spaced approximately 3.5 m apart, as shown in Fig. 2, although only GPR profiles adjacent to the boreholes are discussed in this study. GPR reflection data collection parameters included an antenna separation of 1 m, a sampling interval of 0.8 ns, trace spacing of 0.1 m and acquisition of 16 traces at each location (stacks) to improve the signal to noise ratio. CMP profiles were acquired adjacent to borehole locations in order to compare radar velocities estimated using common offset GPR reflection and CMP methods. CMP profiles were collected with identical parameters to the reflection profiles but had an initial antenna separation of 0.6 m.

GPR data were processed using a bandpass filter (15–30–80–240 MHz) to remove low- and high-frequency noise, and an f–k filter (Yilmaz, 1987) to remove steeply dipping diffraction hyperbolae tails associated with metal vine trellises. No amplitude gain functions were applied to the data. All datasets had similar spectral frequency contents, indicating minimal wavelet dispersion due to variable soil water content. The airwave arrival time was picked on all profiles, and then the airwave and groundwave events were removed by subtracting a wavelet calculated from the average amplitude of traces along each GPR profile (Annan, 2002). This was necessary in order remove the high amplitude groundwave contributions, especially where it obscured the reflected events at locations where the reflector is shallow. Two GPR profiles collected during a single field campaign are shown in Fig. 4. These show a concave upward reflection at two-way travel times (TWTTs) relative to the airwave arrival of between 15 and 40 ns. This reflection was considered a good candidate for estimation of VWC from TWTT as it is a continuous,

high amplitude reflection that displayed a consistent geometry over time. Reflector 'picking' was performed by considering the reflection signatures both before and after removal of the air/groundwater events.

CMP profiles of 100 MHz were collected along vine rows adjacent to the borehole locations during each field campaign (Fig. 2). The CMPs were used primarily to identify the airwave and reflection on common offset reflection profiles (Fig. 5a). A typical CMP gather is shown in Fig. 5b and illustrates the linear airwave and groundwave arrivals as well as the hyperbolic reflection arrival. CMP reflection hyperbolae quality was variable because the reflection was not always horizontal (Baker, 1998) and because the large-offset signals arrived at the limit of the signal penetration. Typical CMP velocities were between 0.06 and 0.1 m ns^{-1} (Fig. 6).

3.3. Petrophysical relationships

The total volumetric water content (VWC$_{total}$) and neutron probe counts (NP) from all boreholes were used to calibrate the neutron probe data VWC$_{total}$ was calculated by summing the free VWC, measured from gravimetric analysis of borehole soil samples using (1), and the constituent water (VWC$_{constit}$) using (2). Boreholes augered under both wet and dry conditions were combined in order to ensure calibration over a range of soil moisture conditions (i.e. 0.1–0.5 m^3 m^{-3}). The scatterplot between collocated neutron probe counts and VWC$_{total}$ measurements is shown in Fig. 7, and the resulting calibration equation is given by

$$VWC_{total} = 5.41 \times 10^{-5} \ NP - 0.1079, \qquad (6)$$

which has a correlation coefficient (r^2) of 0.79. When estimating the free water content of the soil from neutron probe logs, the neutron probe counts were converted to VWC$_{total}$ using (6), and then the constituent water content was subtracted following (2) to obtain the free VWC. In our study, VWC refers to the free water content of the soil.

TDR measurements were collected throughout the study area in October 2002 and February 2003, under wet and dry conditions, respectively, using a Soil-Moisture Trase System with two 0.15 m long probes. The average sample volume of the TDR is a cylinder of 750 cm^3 centered on the probes. TDR data were
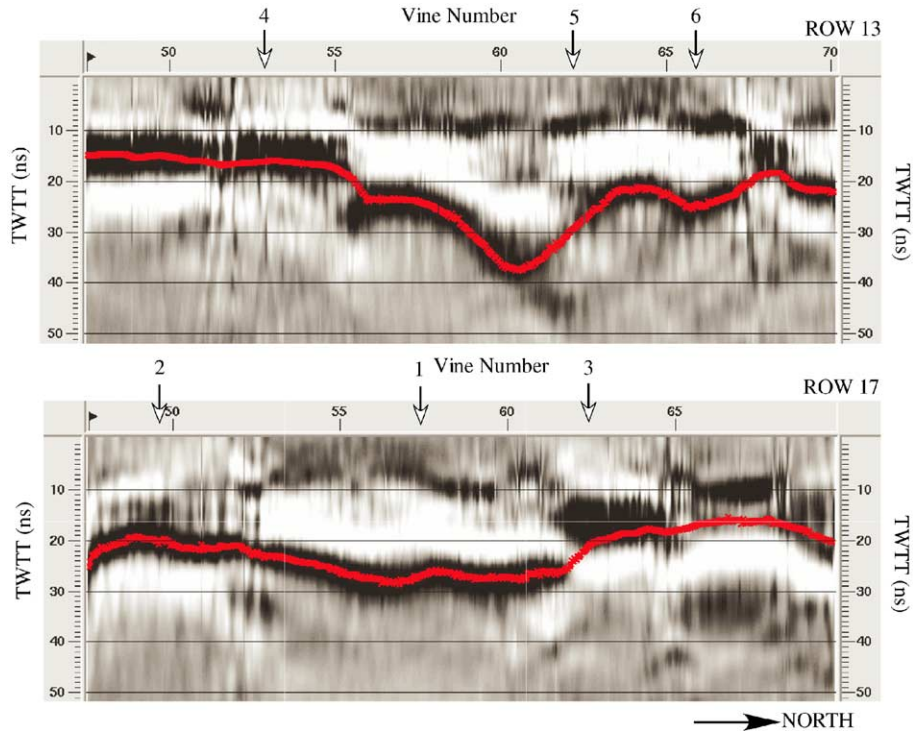
Fig. 4. One hundred megahertz GPR reflection profiles collected adjacent to Rows 13 and 17 (see Fig. 2) in November 2002 after removal of airwave and groundwater events. The travel time picks of the reflection are shown by the grey line. White arrows indicate the position of the numbered boreholes.

collected at the same time as co-located soil samples. GWC and soil textures were measured from the soil samples and were used to develop a site-specific calibration curve between κ (obtained from TDR) and VWC that could be used to estimate VWC from the GPR reflection data as described in Section 2. The calibration data had a higher correlation coefficient (r^2) when fit to the Herkelrath et al., (1991) equation than the Topp et al. (1980) equation. The site-specific calibration curve based on the Herkelrath et al. (1991) equation was

$$\text{VWC} = 0.1168\sqrt{\kappa} - 0.19, \tag{7}$$

with a correlation coefficient (r^2) of 0.84. We observed greater scatter in the wet (February) TDR data, possibly due to water associated with ground-cover vegetation. Although the scale-dependency of the relationship between κ and VWC has not yet been determined, calibration equations developed using TDR measurements collected over decimeter length

scales, have been successfully applied to VWC estimation using GPR over larger length scales (e.g. Weiler et al., 1998; Huisman et al., 2001; Martinez and Byrnes, 2001; Alumbaugh et al., 2002; Grote et al., 2003; Van Dam et al., 2003).

3.4. Estimation of average velocity using GPR reflection method

The two way travel time (TWTT) to the reflection was calculated by subtracting the arrival time of the airwave from that of the reflection on the GPR profile, as shown on Fig. 5a. The airwave and reflection peaks (rather than troughs or zero-crossings) were used for picking travel times as there was minimal interference with adjacent arrivals and they could be consistently identified. To calculate the GPR velocity (v) from the TWTT picks, the time taken for the airwave to travel from the transmitting to receiving antennas, which is the antenna spacing (a) divided by the electromagnetic
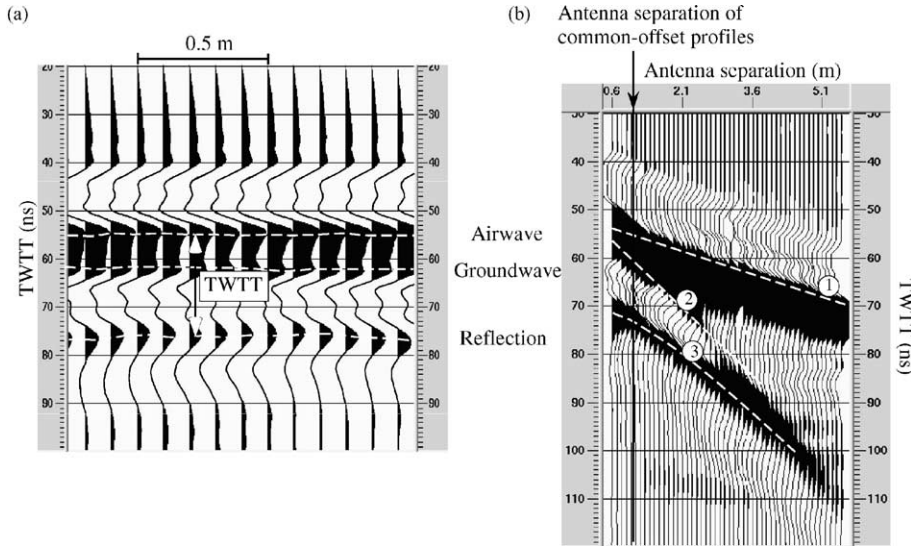
Fig. 5. The common offset profile (a) shows the airwave, groundwave and reflected arrivals, and two-way travel time (TWTT) between airwave and reflected waves used for VWC determination (white vertical arrow). GPR traces are spaced 0.1 m apart. In the CMP profile (b), the linear arrivals (1) and (2) are the airwave and groundwave, respectively, with velocities of 0.3 and 0.1 m/ns. The airwave and groundwave are separated by a TWTT of 6 ns at the antenna spacing used for common offset profiles in fig. a (black arrow), and become more widely separated at larger antenna spacings. The hyperbolic arrival (3) is due to the GPR reflection annotated on fig. a.

wave velocity in air (c), must be added to the difference in TWTT between the airwave and reflection peak. Also, the distance traveled by the wavefront is not simply the depth to the reflector (d), but is a diagonal path determined using the antenna separation distance (Fig. 1). Following Huisman et al. (2003), the GPR velocity (v) can be calculated from TWTT picks using:

$$v = \frac{2\sqrt{d^2 + (0.5a)^2}}{\text{TWTT} + (a/c)}, \qquad (8)$$

The radar wave velocity obtained using (8) was converted to dielectric permittivity using (3), and then converted to VWC using (7).

4. Estimation of VWC under steady state moisture conditions

In the first part of this study, we obtain VWC estimates using GPR reflection profiles that were collected along rows adjacent to the borehole locations (Rows 13 and 17) under steady state soil moisture conditions (i.e. when there was very little vertical water movement through the soil profile). To assess the accuracy of the GPR reflection method, the

results were compared with average VWC measurements from neutron probe logs in the adjacent boreholes (Fig. 2).

4.1. Identification of GPR reflection

GPR profiles were collected under steady state conditions in October, November, and April (Fig. 3). Fig. 7 shows a 100 MHz GPR profile collected along
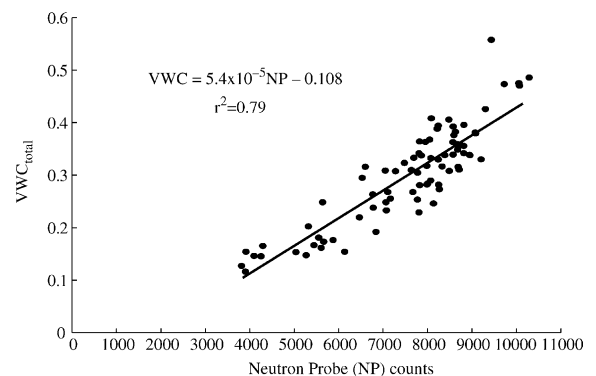

Fig. 6. Site-specific calibration between neutron probe (NP) counts and total volumetric water content (VWC). Data were collected under both dry and wet conditions.
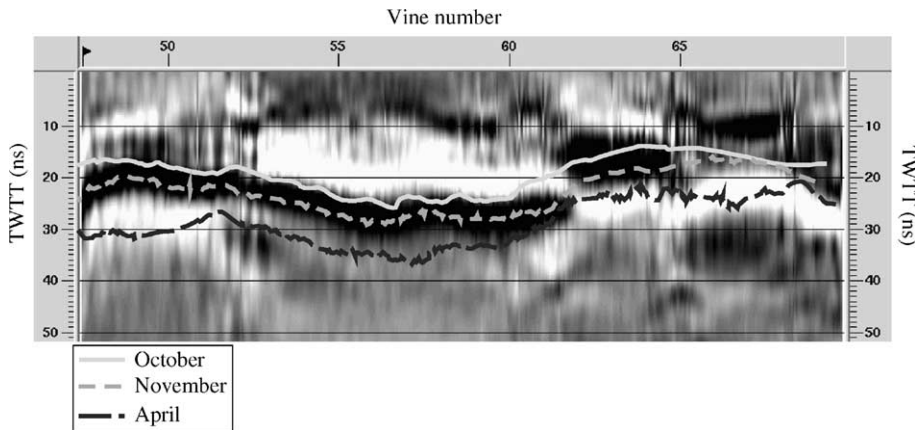
Fig. 7. October and November 2002, and April 2003 travel time picks to reflection on Row 17 GPR profile (see Fig. 3) annotated on the November 2002 GPR reflection profile. Note that the geometry of the reflection is similar under dry and wet conditions. The travel times of the reflection picks increase between October and April as the soil above the reflector becomes wetter.

Row 17 in November with the TWTT of the reflection picks in October, November and April indicated on the same image. The reflector maintains a similar geometry for all months: all GPR profiles reveal a continuous, trough-shaped reflection that occurs between 15 and 50 ns. However, the travel time picks associated with the drier times of the year occur earlier than those of wet times.

The depth of the reflector coincides with a peak in VWC observed on neutron probe logs. An example of VWC from neutron probe logs collected at different times of the year is shown in Fig. 8. Neutron probe logs collected in October show a general increase in VWC from the surface to depths of 0.8–1.3 m (indicated by black arrow on Fig. 8). Neutron probe logs collected in November show a general decrease in VWC near the surface and then increase to a VWC peak at the same depths as the peaks observed on the October neutron probe logs. Under wet conditions, the April neutron probe logs show an increase in VWC to a peak at the same depth as in October and November neutron probe logs. The depth of the shallowest peak in VWC on these logs is consistent under both dry and wet soil moisture conditions. We interpret the reflection seen on the GPR profiles to be caused by the VWC peaks observed on neutron probe logs, associated with a geological horizon.

In order to investigate the origin of the reflector, the weight percent of gravel, sand, silt and clay were measured in the boreholes and compiled into vertical logs. An example of soil texture data at a single borehole is given in Fig. 9. Although we observed some sharp increases in clay and gravel content and an associated decrease in sand content with depth, these texture trends were difficult to extrapolate between boreholes and did not occur at the same depths as the reflector. These soil texture logs are based on 0.1 m long sediment samples collected in the boreholes every 0.33 m, and so soil layers thinner than ∼0.15 m could not be detected. It has been shown that a lithological surface only 0.05 m thick, such as a clay drape, can reduce the vertical water flux and increase the VWC immediately above clay drapes (Judy et al., 1991). However, such thin drapes are unlikely to be detected using our soil texture logs. We collected undisturbed soil cores through the reflecting horizon to qualitatively assess the soil penetration resistance. A combination of augering and vibracore drilling (Smith, 1998) indicated the presence of a thin (0.1 m), cohesive, clay-rich layer at the same depth as the peak in VWC water content and the reflector. Water infiltration tests performed in conjunction with drilling revealed that this layer had much lower permeability than adjacent soils. These field tests confirmed the presence of a thin, clay-rich, low-permeability soil layer that reduced vertical water infiltration at our study site.

The thin, low-permeability clay layer inhibited vertical water flow causing a high VWC above
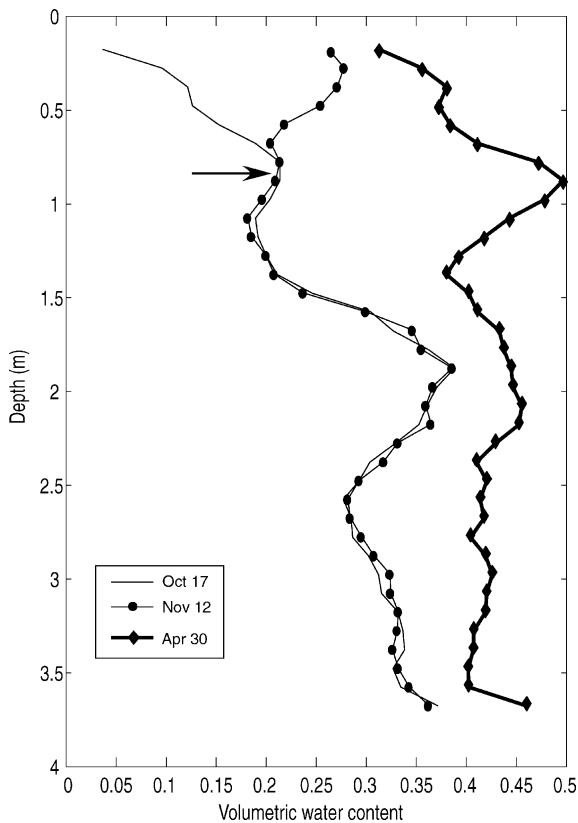
Fig. 8. Neutron probe logs converted to VWC in Borehole 4 (see Fig. 2 for borehole location). October and November logs are distinctly drier than the April log. The black arrow shows the shallow VWC peak associated with the reflector detected on the October, November and April GPR profiles. The water table is below the bottom of the borehole.

the clay layer and lower VWC below the clay layer during October, November and April campaigns. The geological horizon texture contrasts alone did not produce a GPR reflection because it is much thinner than the GPR wavelength, and the difference in dielectric constant between the clay layer and surrounding sediment is not large. However, following (5), the change in VWC across the layer resulted in a larger positive reflection coefficient, with greater thickness than the geological layer, and centered at the location of the clay layer. The decrease in VWC across the clay layer gives rise to a peak on the GPR reflection profiles, similar to the synthetic models of Dai and Young (1997). The peak in VWC observed on the neutron probe logs is at the same depth as the clay
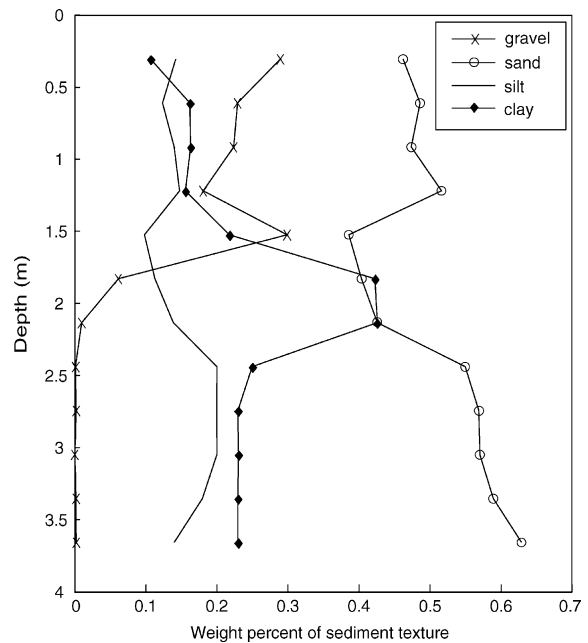

Fig. 9. Sediment texture logs from borehole 4.

layer, although it is somewhat smoothed due to the large sample volume of the neutron probe relative to the thickness of the high VWC layer.

4.2. VWC estimation at the borehole locations

Neutron probe estimates of VWC acquired from boreholes 1–6 in October, November and April were compared with VWC estimates from GPR profiles collected along rows 13 and 17 at the same time The GPR profiles along rows 13 and 17 are located 1.75 m west of the boreholes (Fig. 2). The shallow peaks in VWC (such as those shown on Fig. 8) were used as estimates of the reflector depth (Table 1). The depth of the reflector and corrected TWTT picks to the reflector at each borehole location were subsequently used to calculate the radar wave velocity of the soil layer overlying the reflector following (8). The site-specific Herkelrath Eq. (7) was then used to calculate the depth-averaged VWC at each of the six borehole locations, which were compared with the average VWC estimates to the reflector obtained using neutron probe data, and Eqs. (6) and (2). The main sources of error in VWC estimation are due to scatter in the data

Table 1
Summary of the depths and estimates of average VWC (in $m^3 \, m^{-3}$) in each borehole determined from the October, November and April GPR and neutron probe (NP) datasets

	Borehole #	Reflector depth (m)	VWC (GPR)	VWC (NP)	VWC difference
OCTOBER	1	1.35	0.154	0.127	0.027
2002	2	1.05	0.114	0.100	0.014
	3	0.80	0.168	0.181	-0.013
	4	0.85	0.118	0.087	0.031
	5	1.30	0.140	0.137	0.003
	6	1.15	0.144	0.137	0.007
NOVEMBER	1	1.35	0.181	0.174	0.007
2002	2	1.05	0.172	0.147	0.025
	3	0.80	0.237	0.224	0.013
	4	0.85	0.162	0.182	-0.020
	5	1.30	0.169	0.179	-0.010
	6	1.15	0.176	0.172	0.004
APRIL	1	1.35	0.299	0.324	-0.025
2003	2	1.05	0.312	0.328	-0.016
	3	0.80	0.308	0.316	-0.008
	4	0.85	0.290	0.322	-0.032
	5	1.30	0.326	0.330	-0.004
	6	1.15	0.301	0.304	-0.003

Shaded data are located within the region of low vine vigor. The overall RMS error for all three campaigns was 0.018 $m^3 \, m^{-3}$.

used to develop Eq. (7), and the sampling intervals of neutron probe logs and GPR data. Repeated GPR profiles along the same vine row under identical conditions had an RMS error in TWTT picks of 0.05 ns, indicating that TWTT estimates are highly reproducible. Due to the neutron probe sampling interval of 0.1 m, reflector depths are expected to be accurate to within 0.05 m. Errors associated with these measurements were determined using a first-order error propagation analysis (Ang and Tang, 1975) and are included in the RMS error of VWC estimates described below.

The October VWC estimates were compared with the estimates of VWC derived from neutron probe measurements (Table 1), which were arithmetically averaged between the surface and the depth of the reflector. Estimates of VWC from October GPR reflection data ranged from 0.114 to 0.168 $m^3 \, m^{-3}$, and the VWC estimates from neutron probe logs ranged from 0.087 to 0.181 $m^3 \, m^{-3}$. The maximum difference between neutron probe and GPR estimates of VWC was 0.03 $m^3 \, m^{-3}$, and RMS error for the October data was 0.018 $m^3 \, m^{-3}$.

Around 7 cm (3 in.) of rain fell immediately before collection of the November data (Fig. 3). The infiltration of rainwater increased the soil water content in the top 0.5 m of the soil, as seen in November neutron probe logs (Fig. 8), but did not change the VWC profile in deeper parts of the soil profile. The VWC peak that occurs at the same depth as the reflection could still be identified on the neutron probe logs in all boreholes. Using the same depths for the reflector as those used with the October GPR data, the TWTT of the November reflection was used to calculate radar velocity following (8) and VWC following (7). The estimates of VWC from the November GPR reflection ranged from 0.169 to 0.237 $m^3 \, m^{-3}$ and the VWC estimated from neutron probe logs ranged from 0.147 to 0.224 $m^3 \, m^{-3}$ (Table 1). The maximum difference between neutron probe and GPR estimates of VWC was 0.025 $m^3 \, m^{-3}$, and RMS error for the November data was 0.015 $m^3 \, m^{-3}$.

In April, GPR and neutron probe logs were collected after an extended period of small amounts of precipitation (Fig. 3). The sharp peaks in VWC (Fig. 8) occurred at the same depths as the GPR reflector under dry conditions. Again, we estimated the average VWC at the borehole locations. Comparison of the GPR-based estimates of VWC and the depth-averaged neutron probe estimates of VWC in April are given in Table 1. The results show that estimates of VWC from April GPR reflections range from 0.290 to 0.326 $m^3 \, m^{-3}$ and the VWC estimated from neutron probe logs ranges from 0.304 to 0.330 $m^3 \, m^{-3}$. The maximum difference between neutron probe and GPR estimates of VWC was 0.032 $m^3 \, m^{-3}$, and RMS error for the April data was 0.019 $m^3 \, m^{-3}$. For all datasets and in all boreholes, VWC estimates from the GPR reflection were within $\pm 0.03 \, m^3 \, m^{-3}$ of the neutron probe VWC estimates, with a RMS error of 0.018 $m^3 \, m^{-3}$.

Error analysis of the three different GPR acquisition campaigns suggests that estimation of VWC using the GPR common offset reflection technique at the borehole locations has similar accuracy to existing GPR methods and, although slightly less accurate than the neutron probe (Evett, 2000), offers the potential to accurately estimate the spatial variability of water content across a study area with decimeter-scale resolution.

Spatial trends in VWC are also evident from the GPR profiles across the study area. In October, the VWC was largest in the central and northern parts of the study area, and smallest at the southern end of

the study area (Table 1 and Fig. 2). Higher VWC values occur in locations with reduced vine vigor, as observed by vineyard managers (Fig. 2). In April, the largest VWC values occurred in central parts of the study area. The corrected TWTT to the GPR reflection also varies across the study area with similar trends observed under dry, intermediate and wet conditions. Fig. 10 illustrates the corrected TWTT to the reflection based on GPR data collected across the entire study area during the October, November and April field campaigns. The largest TWTT to the reflection occurs in the central area, which is also the location of the deepest part of the reflector, the wettest soil moisture conditions, and lowest vigor. Vine roots are typically sensitive to the moisture variations in approximately the upper meter of the soil column (Jackson, 2000), and the estimates of VWC from GPR were measured over a similar depth. This suggests that the region of low vigor may be associated with high moisture content in the top 1 m of the subsurface, which is found in places where reflector is deepest. Recent work has focused on using the GPR reflection signatures, together with the wellbore neutron probe data, to estimate two-dimensional depth-averaged VWC estimates within a Bayesian framework and

over the winery site to guide precision viticulture (Hubbard and Rubin, 2004; Hubbard et al., 2004).

5. Discussion

We have presented a successful case study investigating the accuracy of common offset GPR reflection travel time data for estimating the average volumetric water content between the ground surface and a reflector. VWC estimates were obtained from GPR reflection data under dry, intermediate and saturated soil moisture conditions, and where the reflection was associated with a low permeability clay layer.

Our studies have found that estimates of VWC obtained from GPR reflection travel times are accurate to an RMS error of 0.018 $m^3 \ m^{-3}$ of neutron probe estimates of VWC. However, the technique has some limitations, including:

1. The method requires identification and mapping of a reflector across the study area, which may not be possible if there are no strong vertical contrasts in soil texture or VWC.
2. Estimation of reflector depth is critical for obtaining accurate estimates of VWC. Detailed borehole
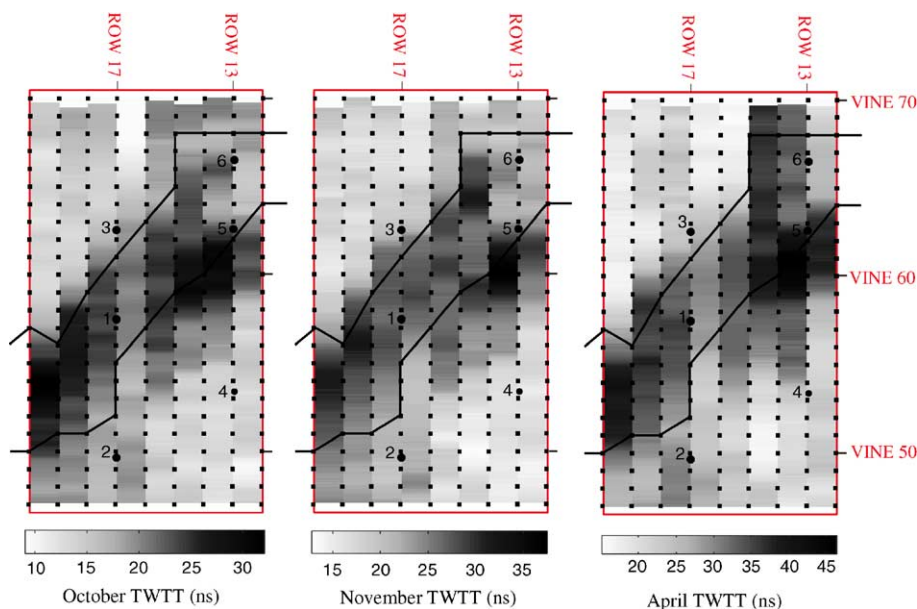

Fig. 10. TWTT to the reflection across the entire study area in October, November and April. The travel time increases between October and April, and the longest travel times are associated with the region of lowest vine vigor, which is bounded by the solid black lines.

information should be used to reduce uncertainty associated with the depth of the reflector(s). The accuracy of VWC estimates are likely to decrease further from the borehole locations.

3. The local hydrologic conditions also influence the suitability of the GPR reflection technique for VWC estimation. In wet climates, heavy rainfall events, which are spaced a few days apart, may result in a transient reflector geometry.

4. Kowalsky et al. (2001) used 2-dimensional synthetic GPR reflection profiles to show that GPR reflection amplitudes vary considerably as a function of soil moisture conditions. This may make the consistent interpretation of a particular reflection event more challenging.

5. Under dry conditions, reflections arrive earlier in time on a GPR profile. Interference of airwave and groundwave energy with reflection arrivals may lead to poor estimates of the travel time to the reflection, and less accurate VWC estimates.

6. Conclusions

This study has focused on assessing the utility and accuracy of surface GPR reflection travel time for VWC estimation under natural conditions and throughout the growing season. Our results have shown that the common-offset GPR reflection method can be used to estimate the average VWC of the soil above a reflecting event with a RMS error of $0.018 \, \mathrm{m^3 \, m^{-3}}$. This method has an accuracy that is comparable with existing conventional methods (i.e. neutron probe, TDR, capacitance probe), and GPR methods. However, as GPR reflection data can be collected rapidly over large areas in a non-invasive manner, this approach offers potential for in situ, high resolution estimates of VWC. Although the GPR reflection and groundwave techniques have similar accuracy and spatial resolution, the reflection technique is able to estimate VWC deeper in the subsurface.

The GPR method relies on the existence of a reflector at known depth. Selecting and verifying the origin and depth of the reflector requires careful attention, and requires detailed borehole information to allow the calibration of GPR reflector depths. This study demonstrated the accuracy of the technique where co-located validation data were available (i.e. at borehole locations). Our study marks the first attempt to quantify the accuracy of common offset GPR reflection travel time for providing estimates of VWC in a naturally heterogeneous environment and under variable hydrological conditions.

References

Alumbaugh, D., Chang, P.Y., Paprocki, L., Brainard, J.R., Glass, R.J., Rautman, C.A., 2002. Estimating moisture contents in the vadose zone using cross-borehole ground penetrating radar: a study of accuracy and repeatability. Water Resource Research 38 (12), 1309.

Ang, A.H-S., Tang, W.H., 1975. Probability Concepts in Engineering Planning and Design: Volume 1—Basic Principles. Wiley, New York p. 409.

Annan, A.P., 2002. Ground Penetrating Radar Workshop Notes. Sensors and Software Inc., PEMD 217, Ont., Canada.

Annan, A.P., 2005. in: Y. Rubin, S. Hubbard (Eds.), GPR methods for hydrogeological studies, Chapter 7 in Hydrogeophysics. Springer (in press).

Annan, P.A., Cosway, W.S., Redman, J.D., 1991. Water table detection with ground penetrating radar, Society of Exploration Geophysicists Annual Meeting, Expanded Abstracts, Houston, USA, pp. 494–496.

Baker, G.S., 1998. Applying AVO analysis to GPR data. Geophysical Research Letters 25 (3), 397–400.

Binley, A., Winship, P., West, J.L., Pokar, M., Middleton, R., 2001. High-resolution characterization of vadose zone dynamics using cross-borehole radar. Water Resource Research 37, 2639–2652.

Chan, C.Y., Knight, R.J., 2001. Determining water content and saturation from dielectric measurements in layered materials. Water Resource Research 35 (1), 85–93.

Clement, W.P., Cardimona, S.J., Endres, A.L., Kadinsky-Cade, K., 1997. Site characterization at the Groundwater Remediation Field Laboratory. The Leading Edge 16 (11), 1617–1621.

Dai, R., Young, C.T., 1997. Transient fields of horizontal electrical dipole on a multilayered dielectric medium. IEEE Transactions on Antennas and Propagation 45 (6), 1023–1031.

Davis, J.L., Annan, A.P., 1989. Ground-penetrating radar for high resolution mapping of soil and rock stratigraphy. Geophysical Prospecting 37, 531–551.

Du, S., Rummel, P., 1996. Reconaissance studies of moisture in the subsurface with GPR, Proceedings of the Fifth International Conference on Ground Penetrating Radar, Kitchener, Ont., Canada, Waterloo Centre for Groundwater Research, vol. 3. University of Waterloo, Waterloo, Ont. pp. 1241–1248.

Evett, S.J., 2000. Some aspects of time domain reflectometry (TDR), neutron scattering and capacitance methods of soil water content measurement, in: Comparison of soil water measurement using the neutron scattering, time domain reflectometry and capacitance methods. IAEA-TECDOC-1137, IAEA, Vienna, Austria pp. 5–49.

Evett, S.R., Steiner, J.L., 1995. Precision of neutron scattering and capacitance type soil water content gauges from field calibration. Soil Science Society of America Journal 59 (4), 961–968.

Ferre, P.A., Knight, J.H., Rudolph, D.L., Kachanoski, R.G., 1998. The sample areas of conventional and alternative time domain reflectometry probes. Water Resource Research 34 (11), 2971–2979.

Fisher, E., McMechan, G.A., Annan, A.P., 1992. Acquisition and processing of wide-apertature ground-penetrating radar data. Geophysics 57 (3), 495–504.

Gardner, W.H., 1986. Water content, in: Klute, A. (Ed.), Methods of Soil Analysis. Part 1. Physical and Mineralogical Methods. Soil Science Society of America, Madison, WI.

Greacen, E.L., Correll, R.L., Cunningham, R.B., Johns, G.G., Nicholls, K.D., 1981. Calibration, in: Greacen, E.L. (Ed.), Soil Water Assessment by the Neutron Method. CSIRO, Australia.

Greaves, R.J., Lesmes, D.P., Lee, J.M., Toksoz, M.N., 1996. Velocity variations and water content estimated from multi-offset, ground-penetrating radar. Geophysics 61, 683–695.

Grote, K., Hubbard, S.S., Rubin, Y., 2002. GPR monitoring of volumetric water content in soils applied to highway construction and maintenance. The Leading Edge 21, 482–485.

Grote, K., Hubbard, S.S., Rubin, Y., 2003. Field-scale estimation of volumetric water content using GPR ground wave techniques. Water Resource Research 139 (11), 1321. 10.1029/2003WR002045.

Herkelrath, W.N., Hamburg, S.P., Murphy, F., 1991. Automatic, real-time monitoring of soil moisture in a remote field area with time domain reflectometry. Water Resource Research 26, 2311–2316.

Hubbard, S.S., Rubin, Y., 2004. The quest for better wine using geophysics. Geotimes 49 (8), 30–35.

Hubbard, S.S., Peterson Jr., J.E., Majer, E.L., Zawislanski, P.T., Williams, K.H., Roberts, J., Wobber, F., 1997. Estimation of permeable pathways and water content using tomographic radar data. The Leading Edge 16, 1623–1630.

Hubbard, S.S., Grote, K., Rubin, Y., 2002. Mapping the volumetric soil water content of a California vineyard using high-frequency GPR ground wave data. The Leading Edge 21, 552–559.

Hubbard, S.S., Lunt, I.A., Grote, K., Rubin, Y., 2004. Vineyard soil water content: mapping small-scale variability using ground penetrating radar, in: Macqueen, R.W., Meinert, L.D. (Eds.), Geoscience Canada Geology and Wine series (submitted for publication).

Huggenberger, P., 1993. Radar facies: recognition of facies patterns and heterogeneities within Pleistocene Rhine gravels, NE Squitzerland, in: Best, J.L., Bristow, C.S. (Eds.), Braided Rivers, vol. 75. Geological Society of London, London, pp. 163–176.

Huisman, J.A., Sperl, C., Bouten, W., Verstraten, J.M., 2001. Soil water content measurements at different scales: accuracy of time domain reflectometry and ground-penetrating radar. Journal of Hydrology 254 (1–2), 48–58.

Huisman, J.A., Snepvangers, J.J.J.C., Bouten, W., Heuvelink, G.B.M., 2002. Mapping spatial variation in surface soil water content: comparison of ground-penetrating radar and time domain reflectometry. Journal of Hydrology 207, 194–207.

Huisman, J.A., Hubbard, S.S., Redman, J.D., Annan, A.P., 2003. Measuring soil water content with ground penetrating radar: a review. Vadose Zone 2, 476–491.

Jackson, R.S., 2000. Wine Science: Principles, Practise, Perception. Academic Press, San Diego.

Johnson, L., Nemani, R., Pierce, L., Bobo, M., Bosch, D., 2000. Toward the improved use of remote sensing and process modeling in California's premium wine industry. Proceedings of IEEE International Geoscience and Remote Sensing Symposium 1, 363–365.

Judy, W.A., Gardner, W.R., Gardner, W.H., 1991. Soil Physics. Wiley, New York p. 328.

Keys, W.S., 1989. Borehole Geophysics Applied to Ground-water Investigations. National Water Well Association, Worthington, OH, p. 313.

Knoll, M.D., 1996. A petrophysical basis for ground-penetrating radar and very early time electromagnetics; electrical properties of sand-clay mixtures. PhD thesis, University of British Columbia, Canada.

Kowalsky, M.B., Dietrich, P., Teutsch, G., Rubin, Y., 2001. Forward modeling of ground-penetrating radar data using digitized outcrop images and multiple scenarios of water saturation. Water Resource Research 37 (6), 1615–1625.

Martinez, A., Byrnes, A.P., 2001. Modeling dielectric-constant values of geologic materials; an aid to ground-penetrating radar data collection and interpretation. Bulletin of the Kansas Geological Survey 247 (1), 16.

Miller, V.C., 1972. Soil Survey of Sonoma County, California, USDA Soil Survey. US Gov. Printing Office, Washington, DC, p. 188.

Peterson Jr., J.E., 2001. Pre-inversion corrections and analysis of radar tomographic data. Journal of Environmental and Engineering Geophysics 6, 1–18.

Powers, M.H., 1997. Modelling frequency-dependent GPR. The Leading Edge 16 (11), 1657–1662.

Roth, K., Schulin, R., Fluhler, H., Attinger, W., 1990. Calibration of time domain reflectometry for water content measurement using a composite dielectric approach. Water Resource Research 26, 2267–2273.

Sakaki, T., Sugihara, K., Adachi, T., Nishida, K., Lin, W., 1998. Application of time domain reflectometry to determination of volumetric water content in rock. Water Resource Research 24 (10), 2623–2631.

Saxton, K.E., Rawls, W.J., Romberger, J.S., Papendick, R.I., 1986. Estimating generalized soil water characteristics from texture. Soil Science Society of America Journal 50 (4), 1031–1036.

Smith, D.G., 1998. Vibracoring: a new method for coring deep lakes. Palaeogeography, Palaeoclimatology, Palaeoecology 140, 433–440.

Stoffregen, H., Zenker, T., Wessolek, G., 2002. Accuracy of soil water content measurements using ground penetrating radar: comparison of ground penetrating radar and lysimeter data. Journal of Hydrology 267, 201–206.

Tillard, S., Dubois, J.-C., 1995. Analysis of GPR data: wave propagation velocity determination. Journal of Applied Geophysics 33, 77–91.

Topp, G.C., Davis, J.L., Annan, A.P., 1980. Electromagnetic determination of soil water content: measurements in coaxial transmission lines. Water Resource Research 16, 574–582.

Tsoflias, G.P., Halihan, T., Sharp Jr., J.M., 1999. Monitoring pumping test response in a fractured aquifer using ground-penetrating radar. Water Resource Research 37 (5), 1221–1229.

Ulrikson, C.P.F., 1982. Application of impulse radar to civil engineering. PhD thesis, Lund University of Technology, Sweden.

Van Dam, R.L., Schlager, W., 2000. Identifying the causes of radar reflections using time-domain reflectometry and sedimentological analyses. Sedimentology 47 (2), 435–449.

Van Dam, R.L., Van Den Berg, E.H., Schaap, M.G., Broekema, L.H., Schlager, W., 2003. Radar reflections from sedimentary structures in the vadose zone, in: Bristow, C.S., Jol, H.M. (Eds.), Ground penetrating radar in sediments: applications and interpretation Geological Society Special Publication No. 211, pp. 257–273.

Van Overmeeren, R.A., Sariowan, S.V., Gehrels, J.C., 1997. Ground penetrating radar for determining volumetric water content: results of comparative measurements at two sites. Journal of Hydrology 197, 316–338.

Weiler, K.W., Steenhuis, T.S., Boll, J., Kung, K.-J.S., 1998. Comparison of ground penetrating radar and time domain reflectometry as soil water sensors. Soil Science Society of America Journal 62, 1237–1239.

Western, A.W., Grayson, R.B., 1998. The Tarrawarra data set: Soil moisture patterns, soil characteristics, and hydrological flux measurements. Water Resource Research 34 (10), 2765–2768.

Yilmaz, O., 1987. Seismic Data Processing. Society of Exploration Geophysicists, Tulsa, OK.